Def Sci J, Vol 36, No 2, April 1986, pp 221-242

Rationalization of the Mechanical Properties of Alpha-Beta *Ti-Mn* Alloys

HAROLD MARGOLIN
Departmeut of Physical & Engineering Metallurgy
Polytechnic Institute of New York, USA

Received 30 January 1986.

Abstract. The behaviour of yield strength, tensile strength, tensile ductility, **Bauschinger** behaviour, fatigue life and crack propagation has been examined in a series of binary *Ti-Mi* alloys, all heat treated to give the same composition of α and β phases. Since the composition of the α and β phases were fixed in each of the alloys, properties depended on morphology, size and distribution, volume fraction, strength and slip characteristics of the individual phases and, in the case of crack propagation, texture. It has been possible to rationalize mechanical behaviour in terms of these variables.

1. Introduction

A number of investigations have been carried out on the tensile' **fatigue**[2-4], **Bauschinger**[5] and'crack **propagation**[6] and tensile fracture[7] behaviour of α=β ***Ti-Mn*** alloys, given essentially the same final heat treatment. Thus, the properties of the alloys studied ***are*** effectively independent of the composition of the ***a*** and β phases but dep nd rather on the size, distribution and morphological features of the microstructures. Recently, a finite element method (FEM) **study**[8,11] has permitted the stress-strain curves of a series of α=β ***Ti-Mn*** alloys with different volume fractions of phases to be calculated*. In addition, the strain distribution between the a and β phases was predicted and found in two cases to be within 4% of the experimental value and within 30% of the experimental value in a third **case**[10]. The observed difference in strain distribution between the a and β phases together with other observations has permitted considerable understanding of the behaviour of α=β ***Ti-Mn*** alloys to be developed. It must be kept in mind that the rationalization to be presented holds specifically for the slip behaviour and strength characteristics of the α and β phases of the *Ti-Mn* system. The discussion and conclusions to be presented may well have to be modified where the slip behaviour

and strength of the two phases differ significantly from the slip behaviour and strength of the **Ti-Mn** α and β phases.

2. Tensile Properties

2.1 *Experimental Observations of Yield and Tensile Strengths*

The tensile properties of α-β *Ti-Mn* alloys were first reported by **Holden,** Ogden & Jaffee' (Fig. 1). These results were subsequently verified by Ankem & Margolin[1]:

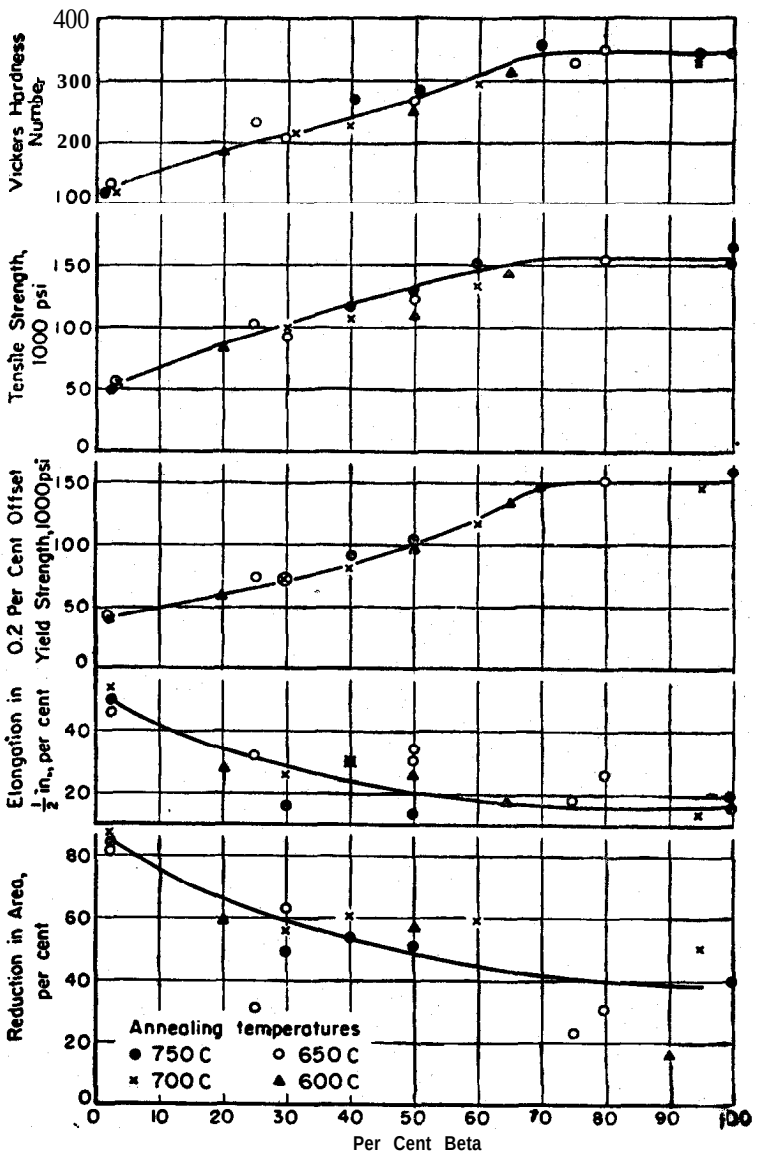

Figure 1. Correlation of tensile properties with retained β content of Ti-Mn alloys annealed at 750°, 700°, 650" and 600°C.

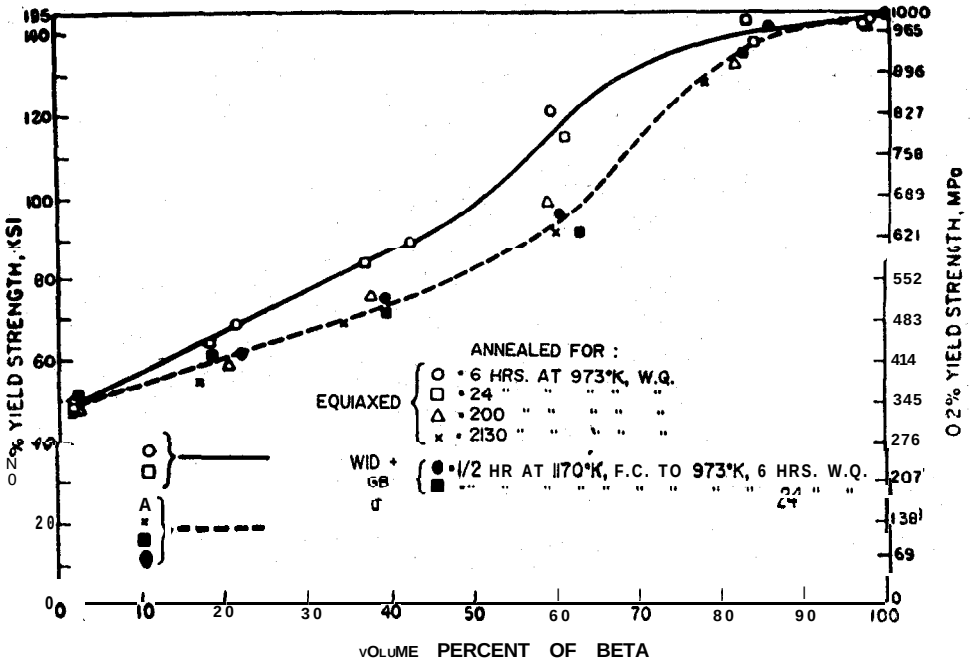

Figure 2a. 0.2% Y. S. as a function of volume percent of β for equiaxed and Widmanstatten plus grain boundary α structures.

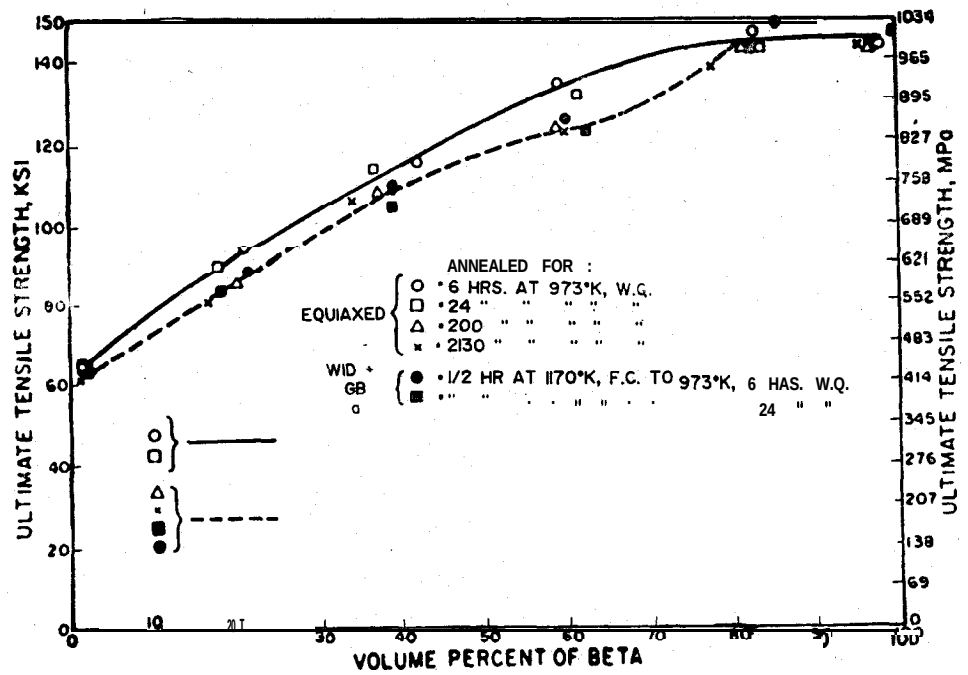

Figure 2b. Ultimate tensile strength as a function of volume percent β for equiaxed and Widmanstalten plus grain boundary α structures.

(Fig. 2a 2b 2c). There are twointere sting features to note in Fig. 1, which refers to equiaxed structures. The yield strength (Fig. 1), increases up to about 70 volume per cent of β after which it remains constant. This is not law of mixtures behaviour. The second point is that the ductility initially drops as *Mn* and the volume per cent of α increases. The ductility subsequently remains essentially constant up to 100 volume per cent β. In this realm of constant ductility, the yield strength increases by a factor of about 1.5-2 (Figs. 1 & 2). Tensile strength reveals characteristics similar to yield behaviour.

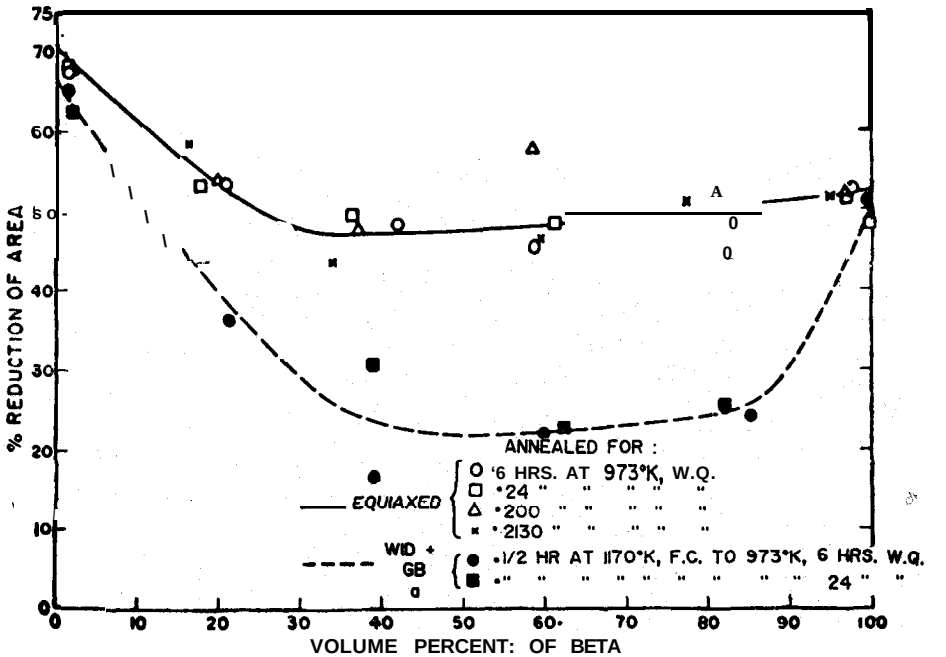

Figure 2c. Reduction of area as a function of volume per cent of β for equiaxed and Widmanstatten plus grain boundary a structures.

In an attempt to explain yield behaviour, FEM calculations have been carried out[8,10]. A two dimensional mesh which was used to simulate the upper half of a tensile specimen is shown in Fig. 3. The dark areas representing α_s constitute 16.3 volume per cent of the structure. The calculated stress and strain distributions along the line G-G which passes through an α particle, are shown in Figs. 4 & 5[10]. The position of the other α particles adjacent to the line G-G should be noted, one below the line to the left and the other above the line and to the right. Stress distributions are shown in Fig. 4 for two applied stress levels, I 10 ksi (758Mpa) and 120 ksi (827 Mpa). The upper diagram refers to stress in the direction of the applied load, σ_y and the lower diagram refers to stresses in the transverse direction, σ_x. The behaviour of the stress distribution is the same for both stress levels and, therefore, let us consider

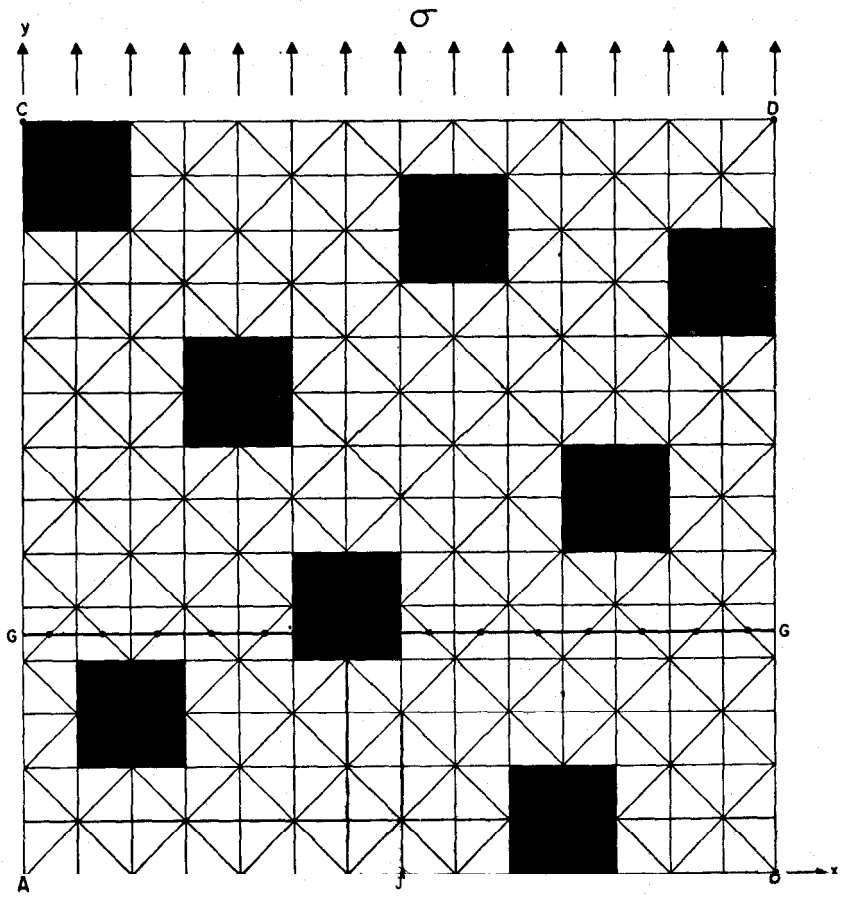

Figure 3. Mesh 1, coarse a particles (16.3 Vol. pct.) shaded in β matrix[8].

only the 120 ksi (827 MPa) stress level. The yield stress of the a is 48 ksi (33 1 MPa), the yield stress of the β is 145 ksi (999 MPa) and the yield stress of the alloy is 135 ksi (930 MPa). Thus the higher applied stress is below the yield stress of the alloy.

Consider the σ_y stresses. The stress levels are higher in the β than in the a, and the β stresses are not symmetrically distributed. The stress in a is approximately 70 ksi (482 MPa). At the left side of the *a* particle the stress in β is 175 ksi (1206 MPa), and it decays to about 100 ksi (689 MPa) just above the a particle at the left of Fig. 3 and then rises away from the *a* particle. There is a similar distribution of stresses in β to the right of the particle, and the minimum level of stress also occurs in the vicinity of the a particle above the line G-G.

Transverse stresses in a are tensile as are the stress levels in the β immediately adjacent to the Y.. At larger distances away from the α/β interface the stress in the β tends to become compressive. The presence of biaxial stresses in a two dimen-

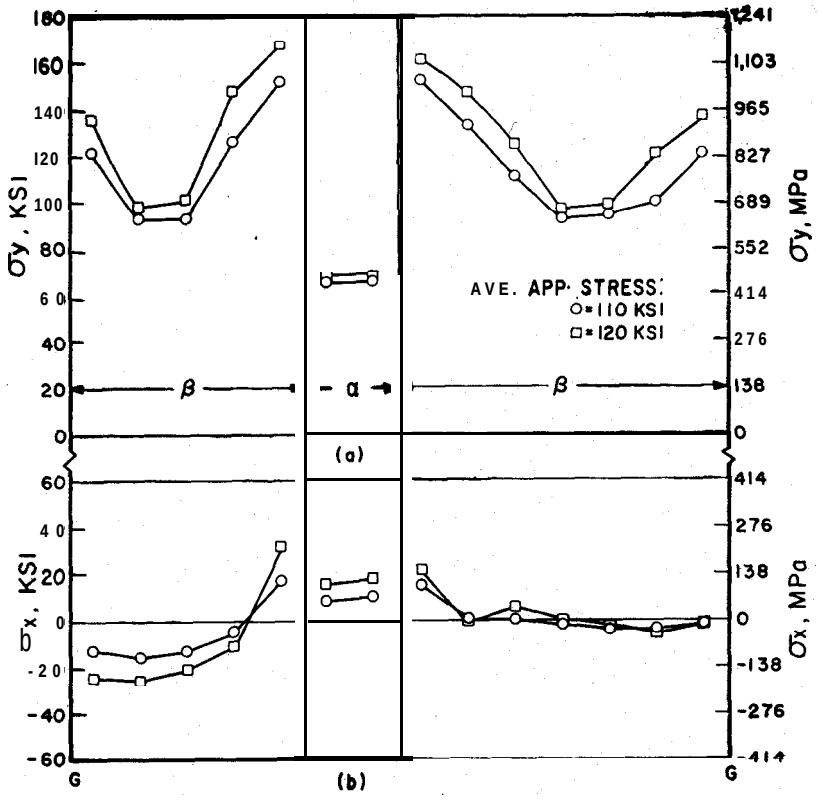

Figure 4. Longitudinal and transverse stress distribution along section G-G of Fig. 3[9].

sional mesh implies that in a three dimensional structure triaxial stresses would develop.

The strain distributions along the line G-G of Fig. 3 are shown in Fig. 5. The strain levels are highest at the centre of the a particle and decrease as they approach the α/β interfaces, where they are the same for each phase, as is required by compatibility conditions. The strain levels in β are highest at the interface where the stresses are also highest. To the left and to the right of the α/β interfaces the strains in β reach a minimum in the vicinity of the *a* particles on either side of line G-G. The strain levels are minimum in β because the strains in the *y* direction are taken up to a greater degree by the adjacent α particles.. Thus, when smaller strains take place in β lower stresses are reached, as was seen in Fig. 4.

From these local stresses and strains it is possible to calculate the average stress and strain in each phase corresponding to an overall stress and strain in the specimen. These calculations are presented[10] in Fig. 6 for an alloy containing 80 vol. per cent a. The input a curve is the lowest curve and the input β curve is the highest curve. The recalculated a and β curves, as well as the calculated overall curve, are given. For a

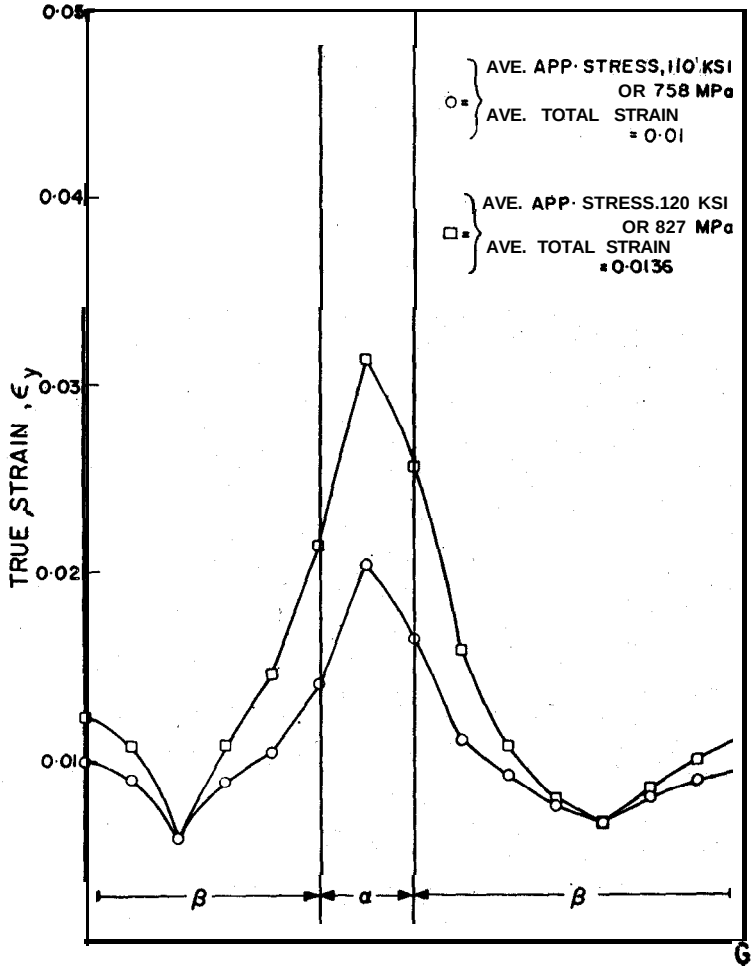

Figure 5. Longitudinal strain distribution along section G-G of Fig. 3[10].

given over all stress and strain, the corresponding stresses and strains in α and β are connected by a tie line. It can be seen that the strains in cc are larger than the strains in β and that the strains in α increasingly exceed the strains in β, as the overall strain level increases.

The calculated ratio[10] of strain in α to strain in β, $\epsilon_\alpha/\epsilon_\beta$, as a function of volume per cent of β is shown in Fig. 7 for coarse particles and in Fig. 8 for fine particles. In both cases there is a minimum in the ratio at 50 volume per cent β. The ratio, $\epsilon_\alpha/\epsilon_\beta$, increases more rapidly from the minimum with decreasing volume per cent of β than with increasing volume per cent of β.

It is important to note that for the finer particle sizes the constraint of the β matrix has reduced the strain ratio, thus bringing the strains in α closer to the strains in β.

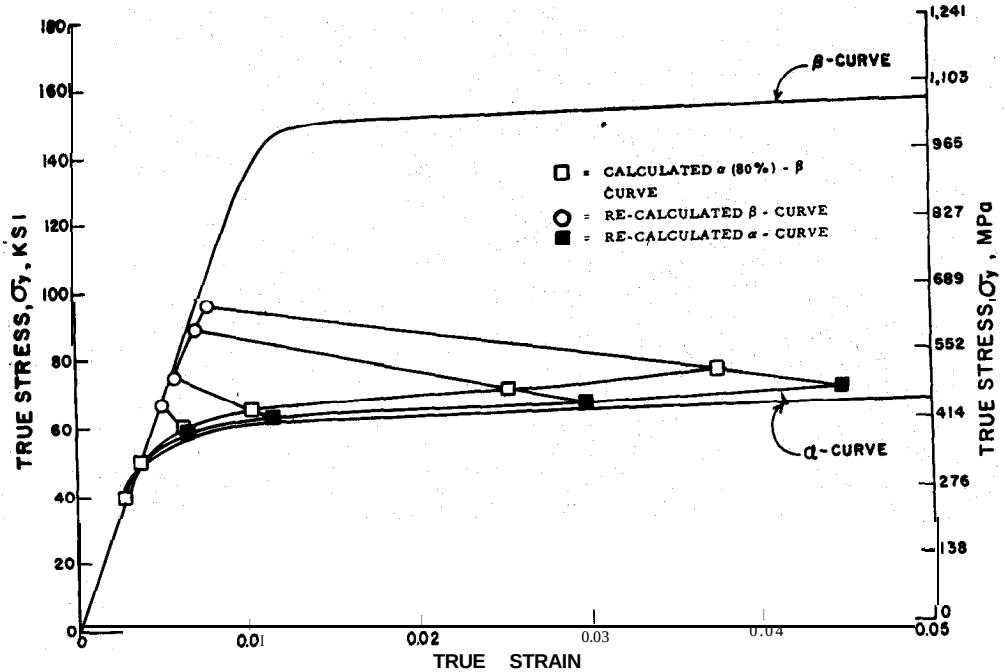

Figure 6. Overall stress and strain distribution for an 80 vol. pct. a (20 pct. coarse β particles) alloy[10].

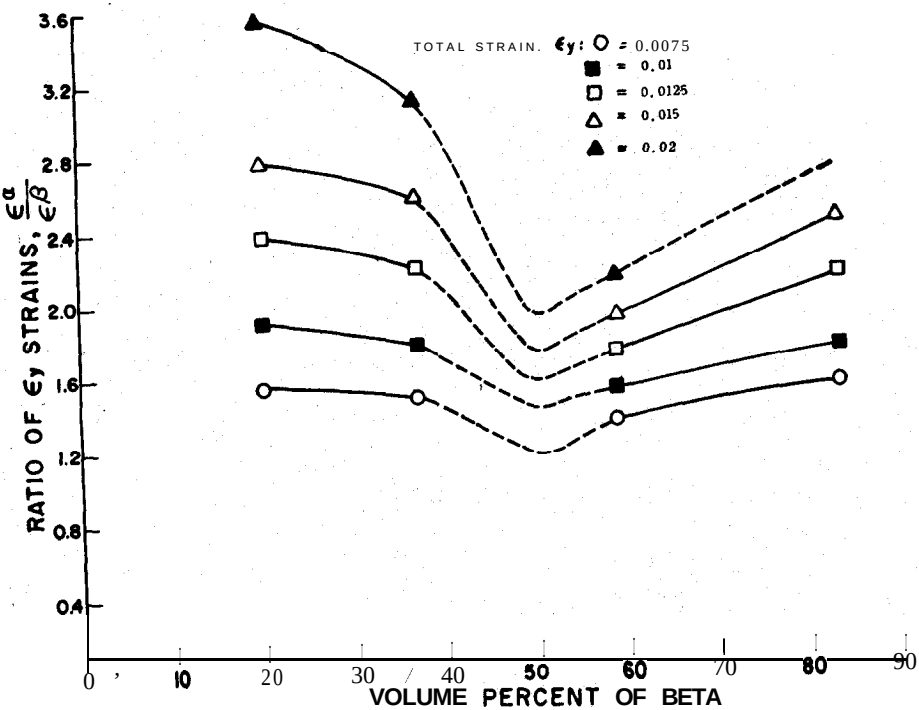

Figure 7. Variation of the strain ratio, $\epsilon_\alpha/\epsilon_\beta$, with vol. pct. β at a series of strains for coarse particles[10].

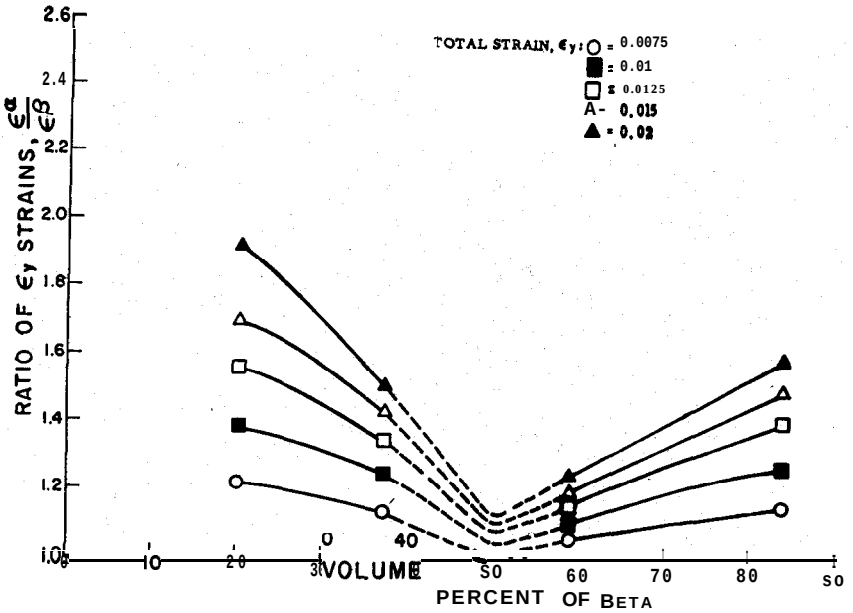

Figure 8. Variation of strain ratio, $\epsilon_\alpha/\epsilon_\beta$, with vol. pct. of β at a series of strains for fine particles'".

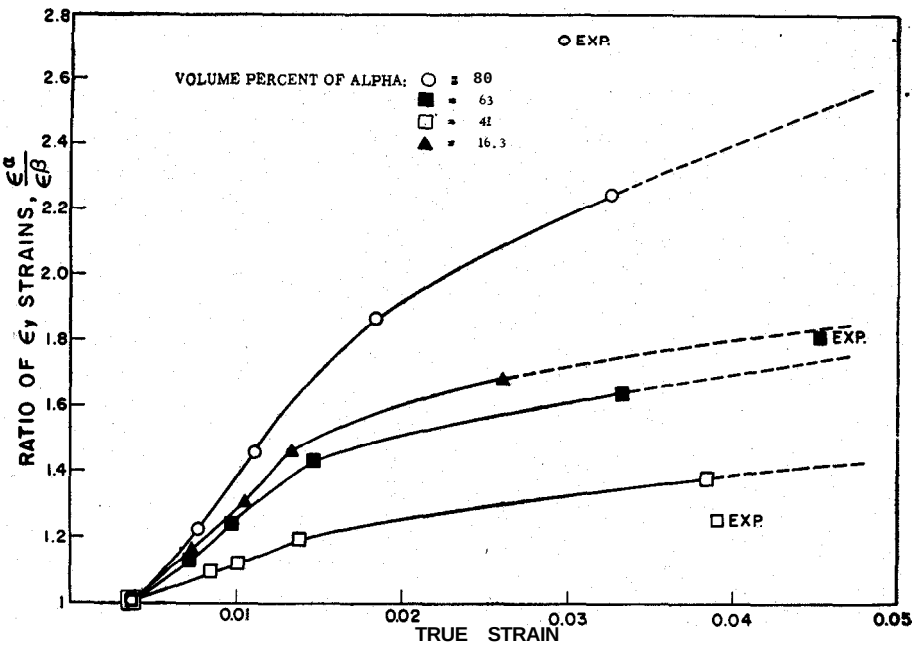

Figure 9. Variation of $\epsilon_\alpha/\epsilon_\beta$ as a function of true strain for α − β alloys with fine particles, directly measured strain distributions for those alloys as shown[10].

The constraint of the β matrix on strain in α is evident in Fig. 5, which shows a smaller strain in α at the interface than within the α particle. It has been possible to check the strain ratios experimentally for 3 alloys, (Fig. 9), by placing a 12μ m square grid of *AZ*

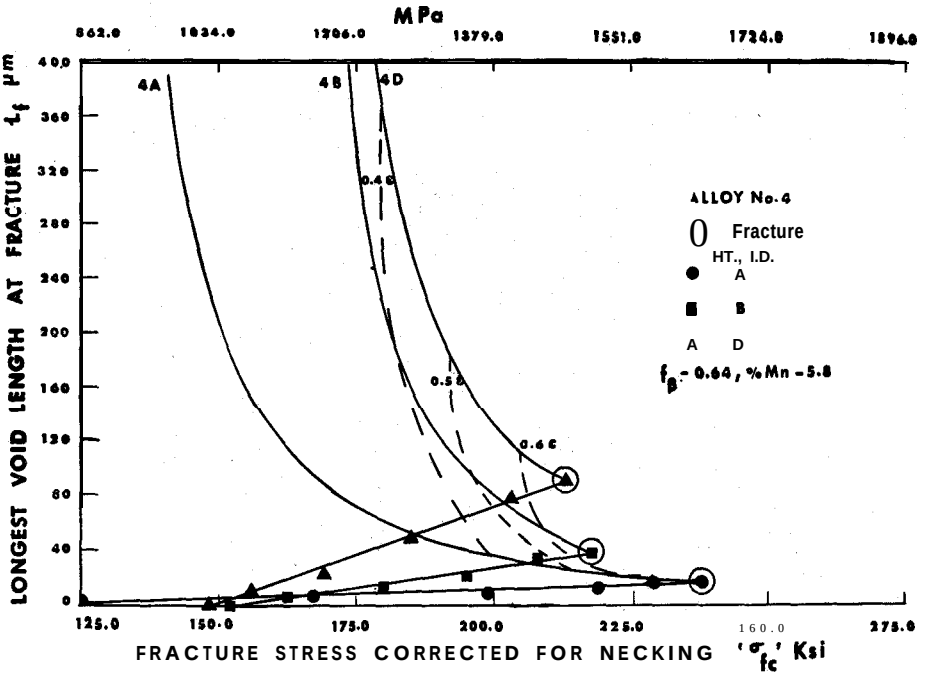

Figure **10a.** Relationship between strain to fracture, critical stress - critical void length and void growth curves for *Ti-5.8Mn*, alloy 4

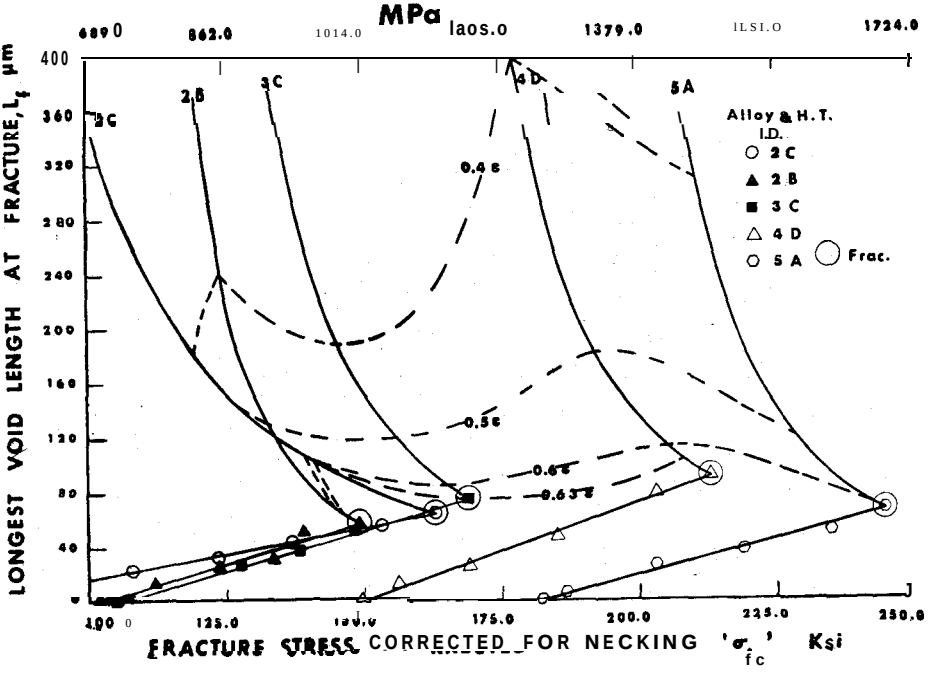

Figure **10b.** Relationship between strain to fracture, critical stress-critical void length, and void growth curves for *Ti*-1.8*Mn* (2B, 2C) *Ti*-3.9*Mn* (3C), *Ti*-5.8*Mn* (4D) and *Ti*-8*Mn* (5A)[7].

lines on coarse structures.* The strains, accompanying plastic deformation of about 3-4.75 per cent, were calculated from the changes in size of the grid. In Fig. 9 the strain ratios in a given alloy are plotted as a function of overall strain in the alloy. As noted earlier, agreement within 4 per cent was obtained in two cases and within 10 per cent in the third instance.

2.2 Proposed Explanation of Yield and Tensile Strength

2.2.1 Yield Strength There are five factors which can be considered to affect yield strength apart from volume fraction of phases. These are :

(a) matrix type,[8] (b) morphology of phases,[9] (c) dislocation density,' (d) size of phases,[10] (e) elastic interaction effects.[11]

If referance to Fig. 2 is made it can readily be seen that a straight line connecting the yield strength of α to the yield strength of β does not fit the data. Such a straight line, as noted, would be a law of mixtures relationship. For the lower curve of Fig. 2a it can be seen that the curve falls between the law of mixtures line for volume per cents of β below 60 per cent and it lies above this law of mixtures line for higher volume per cents of β.

FEM calculations have been carried out to determine the effect of matrix on yield strength of a 50 volume per cent β equiaxed structure alloy. In one instance the matrix was made of α and in the second instance β. It was found that when β was matrix the yield strength was higher.

Although β tends to be matrix above about 40 per cent volume per cent β actual continuity between α particles is not lost until some 60-70 volume per cent of β is present. Thus, for equiaxed alloys the behaviour of a will tend to dominate increasingly below 60 volume per cent β and the yield strength will tend to be below the law of mixtures behaviour. Above 60-70 per cent β the matrix effect will be dominant, and the yield strength will be above the law of mixtures. It has also been observed that the density of dislocations in equiaxed a tends to increase with increasing volume percent of β. This increased dislocation density would add to the β matrix effect.

The coarse equiaxed a structure of Fig. 2a has a considerably lower yield strength than the fine equiaxed α structure. This reduction in yield strength has several sources. First, the coarser α tends to be less constrained by the β matrix, and consequently, flow can take place at a lower applied stress. Secondly, the long annealing times required to develop these coarse structures have undoubtedly strongly reduced the dislocation density. Third, the long slip paths available in the a would tend to promote slip in α more readily to accommodate the greater extent of slip in a permitted by the reduced constraints. This would be mainfested by dislocation pile-ups more effectively causing

* These structures are fine by FEM standards.

slip to develop in a. This point of view is supported by Bauschinger effect studies which show a reduced Bauschinger effect as α particle size increased.'

The Widmanstatten plus grain boundary a structure has yield strengths quite similar to those of the coarse equiaxed structures. However, these yield strengths are achieved for different reasons. It has been shown by examination of the elastic interactions which occur between a and β phases" that elastic strain in β will aid the onset of silp in a. Thus, a smaller applied stress would be required than if no elastic interaction were present. In addition, the Burgers orientation relationship between Widmanstatten α and β matrix produces parallelism between slip systems in the two phases. These slip systems are :

$$(0001)_\alpha \parallel (1\,10)_\beta \quad (1\,\bar{1}00)_\alpha \parallel (1\,\bar{1}\,2)_\beta$$

$$\left[11\bar{2}0\right]_\alpha \parallel \left[1\bar{1}\bar{1}\right]_\beta \quad \left[11\bar{2}0\right]_\alpha \parallel \left[1\bar{1}\bar{1}\right]_\beta$$

Because of this parallelism, slip is more readily transmitted from α to β in the Widmanstätten structure than the equiaxed structure. It is also likely that the dislocation density of *a* in the Widmanstatten structure is below that of the fine α and this contributes to the lower strength of this structure also.

2.2.2 Tensile Strength : An explanation of the tensile strength is more speculative than the rationalization of the yield strength because of fewer data. It is to be anticipated that all of the factors affecting yield strength with the exception of the elastic interaction effects would be operating to affect tensile strength as well. For a given applied strain, the strain in *a* of a two phase alloy is higher than the strain in single phase *a* given the same applied strain. Thus, the dislocation density and strain hardening of α in the two phase alloy will be higher than that of a single phase a. As shown in Fig. 5, the β immediately adjacent to this a experiences high stress and strain. One would anticipate that this behaviour would continue up to the ultimate tensile strength and further that these areas initially adjacent to a would grow in size as the a continued to deform more extensively.

At some point in the deformation it would be expected that the β regions away from the α/β interfaces would begin to deform more than the β adjacent to the interface because of the considerably smaller strain hardening which had occurred. It is proposed that the combination of these effects would produce greater strain hardening than would be found in the single phase deformation of either phase. Comparison of the calculated curve of Fig. 6 with the input curves of the *a* and β phases does, indeed, show higher strain hardening in the alloy than in either phase. This is also manifested in experimentally determined stress-strain curves'.

One would anticipate that the coarse equiaxed structure would not reach the same level of tensile strength as the fine *a* structure, (Fig.- 2b), because of the greater ease of deformation of this a.

2.2.3 Ductility : What is of considerable interest in *Ti-Mn* alloys is that the true strain to fractur eremains constant as the yield strength increased by a factor of about 1.5-2, (Figs. I, 2c). It has been observed in a number of instances[12-14] that tensile fracture occurs when a critical relationship is reached between applied stress and void size, in effect a Griffith type relationship for ductile fracture. The stress and,, therefore, the strain at which fracture takes place is controlled by the rate of void growth. When void growth is rapid the critical stress-critical void size curve[13] is reached at a lower stress and ductility is low. When the void growth rate is slow, the critical curve is reached at a higher stress and ductility is, therefore, higher.

To ascertain the reason for the observed ductility behavior of the *Ti-Mn* alloys it was necessary to establish the critical stress-critical void size curves for each alloy and also to establish the void size vs true stress relationship. As noted above, fracture occurs when the two curves intersect. The critical stress-critical void size curve is established in the following way. For a given alloy, a series of structures with the same true stress-true strain curves are produced. The difference between these structures is only in the extent of the true stress-true strain curves.

For a given structure, the longest void for a particular strain is determined for a number of strains. In all cases the curve is linear, and when it is extrapolated to the fracture strain, the longest void at fracture, L_f, is obtained. The fracture stress at the axis of the specimen, σ_{fc}, can be determined from the measured fracture stress. The plot of L_f vs σ_{fc} is the critical stress-critical void size relationship. The longest void-true strain relationship can be converted to longest void-true stress relationship by substituting the true stress for true strain and the two curves will intersect determining the fracture stress.

When these curves were established for the *Ti-Mn* alloys, it was found that the positions of the two curves shifted in such a way as to maintain ductility very nearly constant. The two curves are shown for a series of *Ti-Mn* alloys' 2(1.8 Mn), 3 (3.9 Mn), 4(5.8Mn), 5(8.0 Mn) in Fig 10[7]. The two sets of curves, by themselves, do not indicate why the strain to fracture should be very nearly the same. To aid in understanding this behaviour constant strain contours have been drawn. Examination of these constant strain contours indicates that fracture occurs at nearly the same strain for each of the alloy series.

3. Bauscbinger Behaviour

The criterion used as a measure of the Bauschinger behaviour was the average Bauschinger strain (ABS). This parameter is defined in Fig. 1 I. The ABS for a series of equiaxed *Ti-Mn* alloys equilibrated at 700°C and strained 1 per cent plastically is given in Fig. 12. It can be seen that the ABS for the 0.025 volume fraction β alloy is about

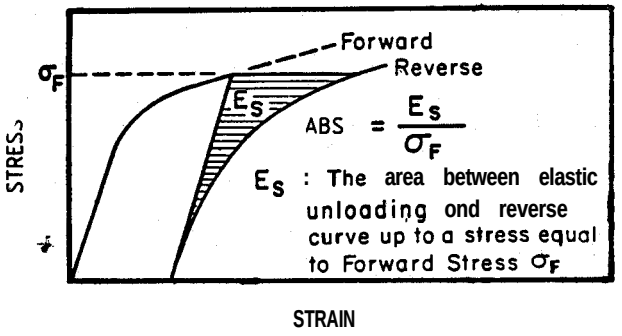

Figure 11. Illustration of procedure for determining average Bauschinger strain (ABS)".

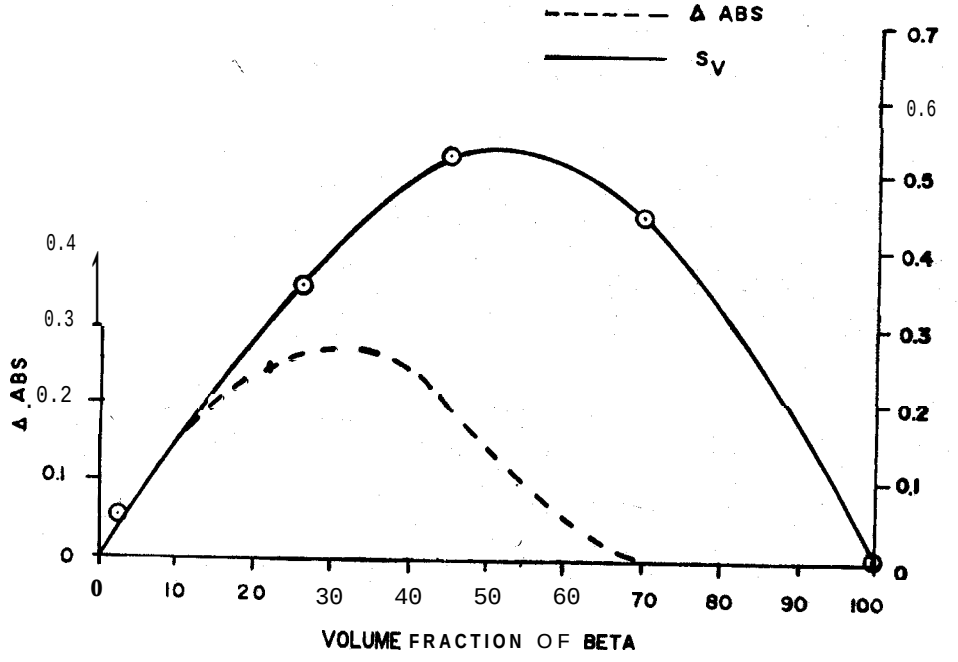

Figure **12.** Difference between average Bauschinger **strain** (ABS) at $\epsilon = 1$ Per cent and rule of mixture ABS curve vs. vol. **pct. β.** Interface area Per **unit volume, Sv, vs. vol.** pct. β **also shown**[5].

3.5 times larger than the ABS of the 1.0 volume fraction β alloy. **It** is also evident that the ABS for the 0.26 and 0.44 volume fraction β alloys is larger than that of the 0.025 volume fraction β alloy. The Bauschinger effect in the 0.025 and 1 .O volume fraction alloys must arise as a result of dislocations which pile-up against the grain boundaries and then move back during reverse flow. The near alpha alloy **hasa** high

strain hardening rate[7] and this is manifested by fine distributed slip[15]. The β alloy reveals coarse slip and low strain hardening[5]. The reverse flow in these two alloys is complicated by stresses introduced as a result of plastic incompatibility at grain or interface boundaries[16], stresses which may extend for a considerable distance from the grain or interface boundary and which may cause new slip on reverse flow[5]. The fine slip in a is an indication of obstacle hardening which would aid reverse flow, while the coarse slip in β is an indication of the opposite behaviour. It was proposd that this coarse slip is a manifestation of the destruction of pre-omega structure[5] formed during quenching.

In the case of the 0.26, 0.44 and 0.69 volume fraction β alloys the Bauschinger behaviour probably arises in large part as a result of the pile-up of dislocations, originating in α, at α/β interfaces. This suggestion is supported by the observation that the ABS in Widmanstltten plus grain boundary α structures is much smaller than that in equiaxed alloys. In the Widmanstatten structures, slip can easily be transferred from the *a* to the β because of the parallelism of the slip systems in the two phases.

As can be noted in Fig. 12, the ABS for the 0.26 and 0.44 volume fraction β alloys lies considerably above the law of mixture lines. One would suspect that the values of the ABS for these two alloys is larger than that of the 0.025 volume fraction β alloy because of strain concentration in a, arising from the presence of β[8, 10]. The trend of the ABS curve of Fig. 12 with decreasing amounts of a is similar to that of $\epsilon_\alpha/\epsilon_\beta$ vs volume fraction of β curve of Figs. 7 and 8. One would, therefore, anticipate that there should be a correlation between $\epsilon_\alpha/\epsilon_\beta$ and ABS. Indeed, such a relationship is shown in Fig. 13.

4. Fatigue Life

Fatigue life of equiaxed and Widmanstätten plus grain boundary α structures have been examined in a series of *Ti-Mn* alloys in which the volume fraction of β varied from 0.025 to 1.0. The tests were carried out with total strain control, with the number of cycles to failure N_f ranging up to approximately 10^4. Fatigue life is primarily controlled by the behaviour of *a-Ti* which deforms first and more extensively than β because α has 1/3 the yield stress of β.

Fatigue life for Widmanstätten structures were lower than those of equiaxed structures, and fatigue life of equiaxed structures were lower the coarse were the equiaxed a particles. In both structures, fatigue crack initiation was primarily associated with α. In the Widmanstltten structures long surface cracks were readily developed along both Widmanstltten and grain boundary a. These long surface cracks propagated only a small distance into the specimen before fracture occurred. Crack nucleation was also easier in the coarser equiaxed structures, and this also led to shorter lives.

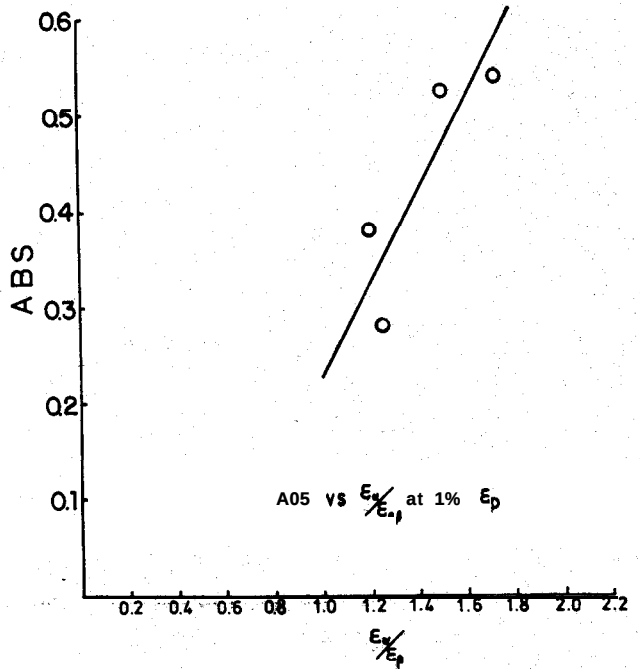

Figure 13. Average Bauschinger strain vs. strain ratio, $\epsilon_\alpha/\epsilon_\beta$.

Crack path measurements in an equiaxed a alloy containing 0.56 volume fraction β revealed that the crack path preferred a and α/β interfaces. The interfaces were increasingly preferred as the particle size and total strain increased[4].

Results of fatigue life tests are usually plotted as number of cycles of failure, N_f, vs. stress, total strain or plastic strain, depending on the control mode of the test. In total strain control, the total strain amplitude $\Delta\xi_{t/2}$ is expressed as the sum of the elastic, $\Delta\xi_{e/2}$, and plastic, $\Delta\xi_{p/2}$, amplitudes. This relationship can be written as[17,18].

$$\Delta\xi_{t/2} = \Delta\xi_{e/2} + \Delta\xi_{p/2} = \frac{\sigma_f}{E}(2N_f)^b + \epsilon_f'(2N_f)^c$$

where σ_f', ϵ_f', b and c are material constants.

This equation is known as the Coffin-Manson equation. By using thisequation, it can be demonstrated that fatigue life is governed by stress for long lives and plastic strain for short lives[19]. A plot of $\Delta\xi_{t/2}$ vs N_f is shown in Fig. 14 for a group of *Ti-Mn* alloys and the relationship between $\Delta\epsilon_{p/2}$ and N_f is given in Fig. 15 for the same alloys. In the vicinity of a plastic strain of 0.004, (Fig. 15), the slope of the curves, which corresponds to the exponent c of the Coffin-Manson expression, passes through a minimum value for alloys 4 and 5. A plot of the absolute value of the exponent c vs the average Bauschinger strain, ABS, is given in Fig. 16.

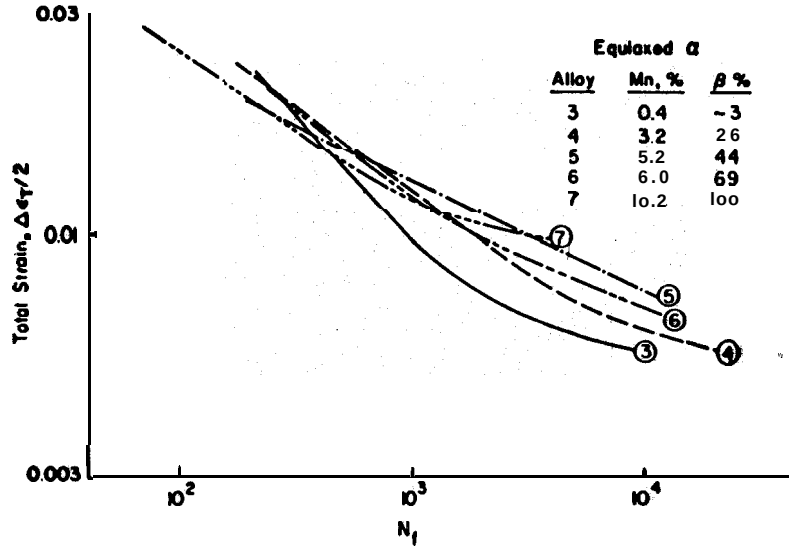

Figure 14. Number of cycles to failure vs. total strain for alloys 3-7[3].

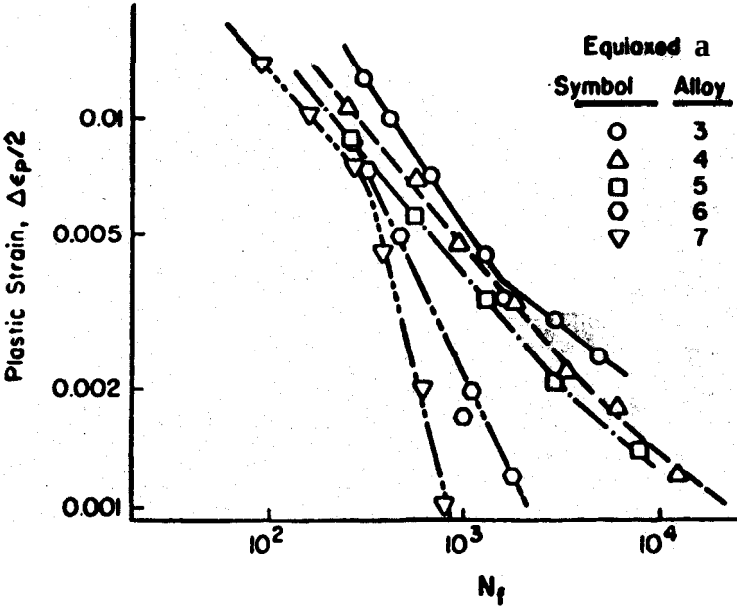

Figure 15. Number of cycles to failure of Fig. 14 as a function of plastic strain[3].

It can be seen that as the value of c decreases the ABS increases. A decrease in the absolute value of c indicates increased plastic resistance to fatigue[20]. Bauschinger strain causes reverse slip[21], and the Bauschinger effect has been proposed as a measure of slip reversibility[22]. If it is considered that crack extension takes place during the

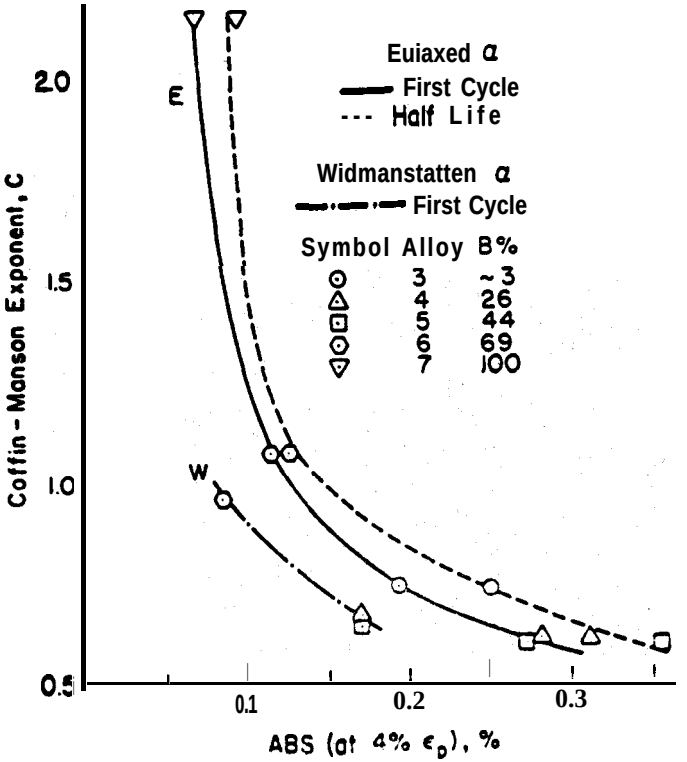

Figure 16. Coffin-Manson exponent C vs. average Bauschinger strain (ABS) at 0.4 pct. plastic strain.

rising part of the load cycle, then the effect of slip reversibility would be to reduce the reversed plastic zone size and to affect the shape of the crack tip, which must in turn affect crack propagation. This observation relating the exponent C and the ABS is also supported by the effect of morphology and particle size on fatigue life. Equiaxed α produces a larger ABS than Widmanstatten α, and finer equiaxed a particle size also yields a larger ABS. Improved fatigue life[3] accompanies these increased ABS values.

5. Fatigue Crack Propagation

Crack propagation has beeu studied with compact tension spedimens in a series of equiaxed α/β *Ti-Mn* alloys containing 0.4, 2.0, 5.6, 8.0 and 10.0% *Mn* with volume fraction of β varying from 0.019 to 0.759 and the crack propagating in the transverse (LT) and longitudinal (TL) directions[23]. Crack propagation rates were found to be a function of texture, yield strength and volume fraction of phases. The role of texture is to orient the phases and in this way to determine which slip systems will operate during crack propagation. Crack propagation rates depend on the total resolved

shear stress determined from the crack tip stress field and the orientation of the operating slip direction with respect to the crack propagation direction. Crack propagation rates were assumed to be highest for that slip system where the product of the total resolved shear stress and the cosine of the angle between the slip direction and the crack propagation direction was highest. This product was labelled the crack propagation factor, CPF. On this basis it was possible to predict that with increasing β-phase the crack propagation in Stage I for the TL direction should move to lower A K values than those encountered in the α phase. The same considerations regarding CPF indicated that at low values of β volume fraction, crack propagation in Stage II should be higher in the LT direction, and in high f_β values crack propagation should be more rapid in the TL direction. These predictions were borne out by the crack propagation data obtained.

Crack propagation data are usually plotted as log A a/AN vs log A K. In this series of alloys the yield stress varies by a factor of 3 as f_β varies from 0.019 to 0.759. Thus, at a given value of A K, one is not comparing crack propagation behaviour for the same yield strength. It is, therefore, necessary to normalize A K on yield stress. The resulting plot of log $\Delta a/\Delta N$ μs log A k/Y S is presented in Fig. 17. It can be seen that, at

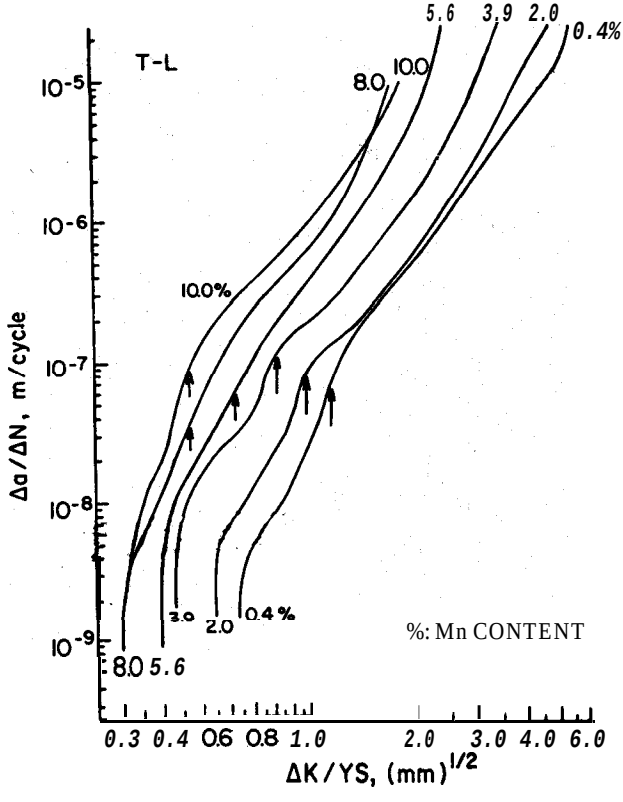

Figure 17. $\Delta a/\Delta N$ as a function of A K/YS for the 0.4, 2.0, 3.9, 5.6, 8.0 and 10.0 *Mn* alloys for the TL direction. Arrows indicate end of Stage I[23].

a given value of A K/Y_S, crack propagation is much more rapid in the high Mn, i.e., high f_β, alloys than in the low f_β alloys. This coincides with the smooth bar specimen data of Fig. 15, which show that high f_β alloys have lower fatigue lives at a given value of $\Delta\epsilon_{p/2}$.

Threshold AK, ΔK^{th}, values as a function of f_β are revealed in Fig. 18. The yield stress of a, as noted earlier, is 1/3 the yield stress of β and, consequently, ΔK^{th} must depend in a major way on slip in α. On this basis, one would expect that, in Stage I, a would show considerably more deformation than β. This is indeed shown in Fig. 19 where a has a rough appearance, and β has the smooth Stage I appearance.

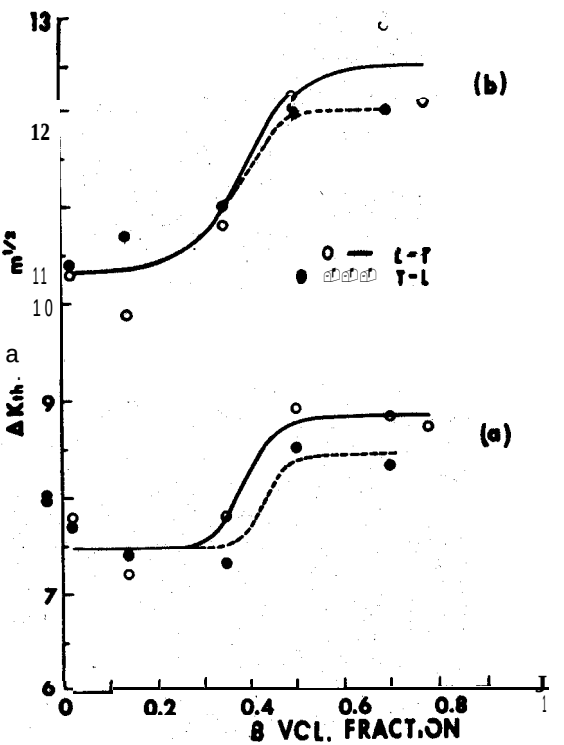

Figure 18. Threshold ΔK, ΔK_{th} (a) for surface and (b) for internally[24] determined ΔK_{th} values as a function of f_β[23].

The marked change in yield strength in the range of $f_\beta = 0.3 - 0.7$, (Figs. 1 and 2), is associated with a change in the matrix from a to β, and a decrease in the continuity of the a phase, which continuity continues despite the fact that β becomes matrix at $f_\beta = 0.35 - 0.4$. When the β phase becomes the matrix, the influence of the α is reduced because of its reduced volume fraction. The matrix must entirely fracture before the crack can advance. Thus, the smaller the amount of a, the greater is the

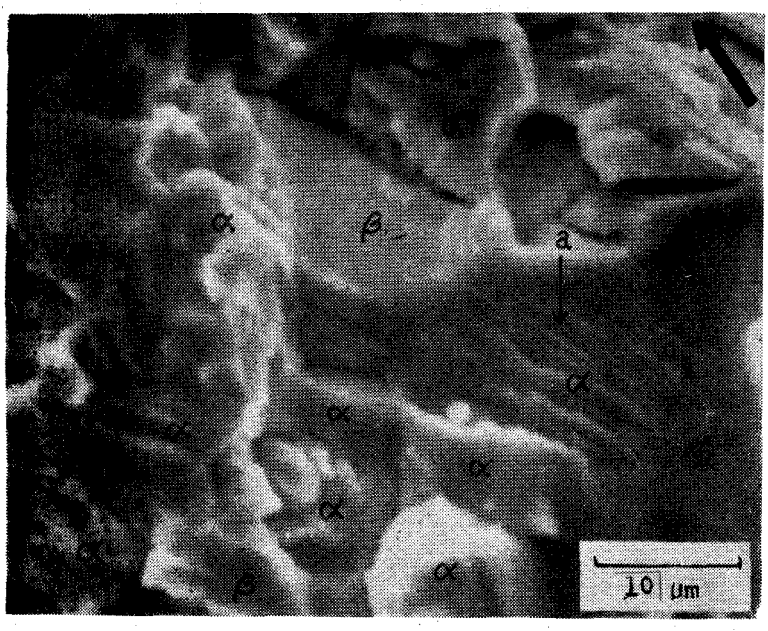

Figure 19. Fractograph of 3.9*Mn* alloy at $\Delta K = 10\text{MPa}\sqrt{m}$, $\Delta K/YS = 0.735\sqrt{mm}$. Stage I, LT direction. Arrow at upper right indicates crack movement direction. Facet like regions are β and rough appearing regions are α, according to EDAX[21].

extent of deformation which β must undergo to produce cracking in α. Because of the reduced influence of α, ΔK_{th} must increase rapidly in the range f_β = 0.3 to 0.7, as does the yield strength.

Finally, it is to consider the possible relationship between striation formation and the Bauschinger effect. Slip in the a phase is quite coarse and localized. As a result it was possible to measure the plastic zone size[25], and it was found that the plastic zone could be detected before striations appeared[23]. Striations appear during reverse plastic flow[26]. Detection of striations requires sufficient reverse flow in order to be seen. Strain hardening in the forward direction limits the extent of the reverse flow on the forward operating slip systems, and this strain hardening must increase with increasing forward flow.

If, in Stage II, the same slip planes and directions, which operate in the forward direction, must operate in reverse flow to cause striations, this will further increase the stresses, formed during unloading, which are required to produce reversed plastic flow. The unloading stresses increase with increasing plastic flow at the crack tip, because they depend on the difference in reverse contraction between elastic and plastic regions, a difference which is, in effect, Bauschinger behaviour. Thus, high f_β alloys which have lower ABS values[5] tend to show less prominent striations[23].

Acknowledgement

The work reported here was sponsored by the Office of Naval Research under contract N-00014-75-C-0793 and Air Force Office of Scientific Research Grants Nos. AFOSR-75-2774 and AFOSR-79-0028. The author is indebted to Drs. Bruce MacDonald (ONR) and Alan Rosenstein (AFOSR) for their encouragement and continued interest. The results discussed here are based on the doctorate work of Y. Saleh, S. Ankem and J.S. Park and the master's study of T.V. Vijayaraghavan. I am indebted to them for their insights, skill and considerable efforts.

References

1. Holden, F. C. Ogden H. R. & Jaffee, R. I. *Trans. AZME, 200* (1954), 169.
2. Saleh, Y. & Margolin, H. *Met. Trans. A,* 11A (1980), 1295.
3. Saleh, Y. & Margolin, H. Met. *Trans. A,* 13A (1982), 1275.
4. Saleh, Y. & Margolin, H. *Met. Truns. A,* 14A (1983), 1481.
5. Saleh, Y. & Margolin, H. *Acta. Met., 27* (1979), *535.*
6. Park, J. S. & Margolin, H. *Met. Trans. A,* 15A (1984), 155.
7. Margolin, H. & Vijayaraghavan, T. V. *Met. Trans. A,* 14A (1983), 2043.
8. Ankem, S. & Margolin, H. *Met. Trans. A,* 13A (1982), 595.
9. Ankem, S. & Margolin, H. unpublished research, (Polytechnic Inst. of New York, Brooklyn, NY), 1980.
10. Ankem, S. & Margolin, H. *Met. Trans. A,* 13A (1982), 603.
11. Ankem, S. & Margolin, H. *Met. Trans.* A, 11A (1980), 963.
12. Greenfield, M. A. & Margolin, H. *Met. Trans., 3* (1972), 2649.
13. Margolin, H. & Mahajan, Y. *Met. Trans. A,* 9A (1978), 781.
14. Margolin, H. &Rosenberg, L. *'Titanium* '80', *Science and Technology',* ed. H. Kimura and 0. Izumi, (TMS-AIME, Warrendale, PA.). 1981, p. 1637.
15. Margolin, H. & Longo, R. *Scripta Met., 13* (1979), 561.
16. Lee & Margolin, H. unpublished research, (Polytechnic Inst. of New York, Brooklyn, NY), 1983.
17. Coffin, L.F. *Trans. ASME, 76* (1954), 931.
18. Manson, S. S. (NASA Technical Notes, Washington, DC.) 1954, p. 2933.
19. Manson, S. S. & Hirschberg, M. H. *'Fatigue: An Interdisciplinary Approach',* (Syracuse University Press, Syracuse, NY.) 1964, p. 133.
20. Peltner, C. E. & Beardmore, P. *ASTM STP* 467, (ASTM, Philadelphia) 1970, p. 77.
21. Charsley, P. & Desvaux, M.N.E. *Mat. Sci. and Eng., 4* (1969), 210.
22. Bothias, C. & Pelloux, R. M. *Met. Trans., 4 (1973).* 1265.
23. Park, J. S. & Margolin, H. Met. *Trans.* A, 15A (1984), 155.
24. *1974 Book of ASTM Standards,* Part 10 E 399-74, p. 432.
25. Park, J. S. & Margolin, H. *Scripta., Met., 17* (1982), 371.
26. Laird, C. 'Fatigue Crack Propagation', *ASTM STP 415,* (ASTM, Philadelphia), 1966, p. 247.